Journal of Zhejiang University-SCIENCE A (Applied Physics & Engineering)

Development of underwater electric manipulator based on interventional autonomous underwater vehicle (AUV)

Xiaohui HU, Jiawang CHEN, Hang ZHOU, Ziqiang REN

Cite this as: Xiaohui HU, Jiawang CHEN, Hang ZHOU, Ziqiang REN, 2024. Development of underwater electric manipulator based on interventional autonomous underwater vehicle (AUV). *Journal of Zhejiang University-SCIENCE A (Applied Physics & Engineering)*, 25(3):238-250.
https://doi.org/10.1631/jzus.A2200621

1. Introduction

- **In applications such as marine rescue, marine science, archaeology, and the offshore industries, autonomous underwater vehicles (AUVs) are frequently used for survey missions and monitoring tasks, with most operations being performed by manned submersibles or remotely operated vehicles (ROVs) equipped with robotic arms.**

Oil and Gas Exploration

Civil Engineering

Marine exploration

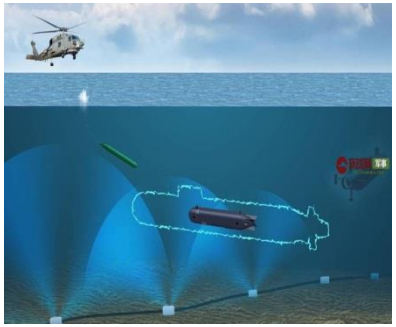

Military applications

- **The electric manipulator arm does not require a hydraulic mechanism, has fewer components, is smaller in size, is easy to mount on lightweight ROVs, and can achieve precise control of force/torque as well as high motion control accuracy.**

2. Architecture of the underwater manipulator

2.1 Manipulator Structure Design

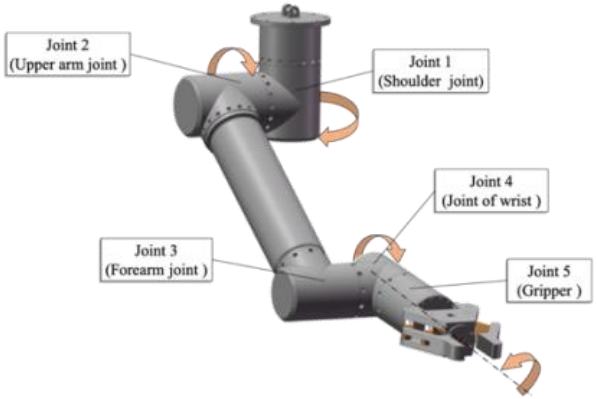

Five-function Electro-manipulator

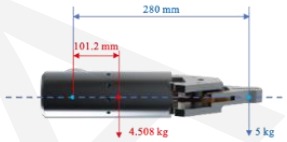

Forearm joint force analysis diagram

Upper Arm Joint Force Analysis Diagram

Manipulator joint motor parameters requirement table

Joint	Shoulder joint	Upper arm joint	Forearm joint	Joint of wrist
Torque in demand	Swing damping	Rotary drive	Rotary drive	Eccentric moment
Maximum arm of force（m）	0.1195	0.667	0.253	0
Maximum driving torque（Nm）	64.6	64.6	19.6	19.6

joint motor parameters

Joint	Rated torque (Nm)	Peak torque (Nm)	Motor power (W)	Peak speed (rpm)
Shoulder joint	52	107	400	30
Upper arm joint	52	107	400	30
Forearm joint	31	70	200	30
Joint of wrist	31	70	200	30
Gripper	7	23	100	60

The manipulator has five degrees of freedom, including one degree of freedom for lifting and four degrees of freedom for rotating the joints, which, together with the opening and closing hand claws at the end, form an overall six-function manipulator.

2. Architecture of the underwater manipulator

2.2 Pressure-balancing device

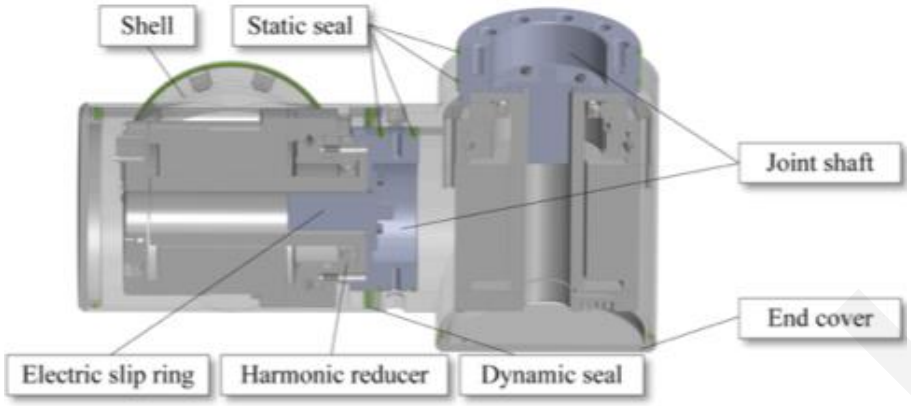

Waterproof design of manipulator joints

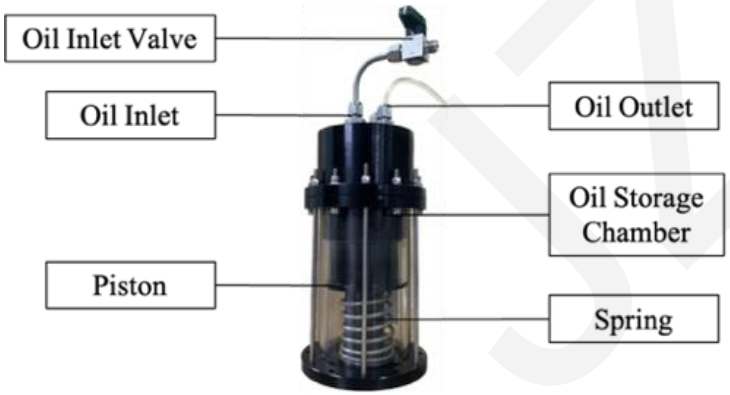

Liquid pressure compensator

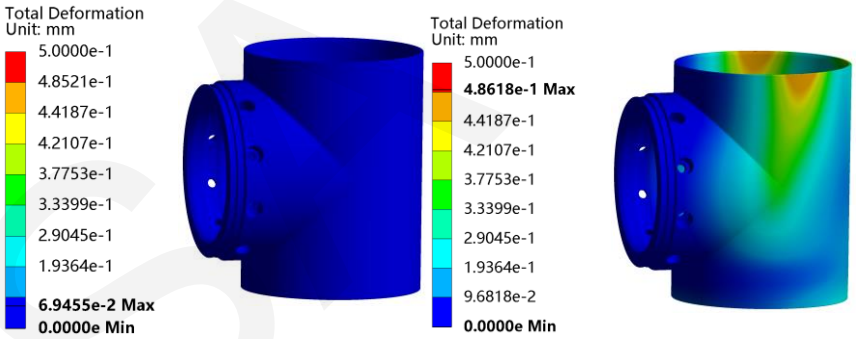

Simulation of pressure resistance of joint housing of manipulator

At a uniform pressure of 1 Mpa, the maximum deformation of the housing is 0.069 mm; at a uniform pressure of 7 MPa, the maximum deformation of the housing is 0.486 mm.

Increased pressure increases the deformation of the housing, leading to seal failure, so the pressure compensation system is designed to increase the water depth at which the manipulator system can be used.

2. Architecture of the underwater manipulator

2.3 Docking method and mechanism design with AUV

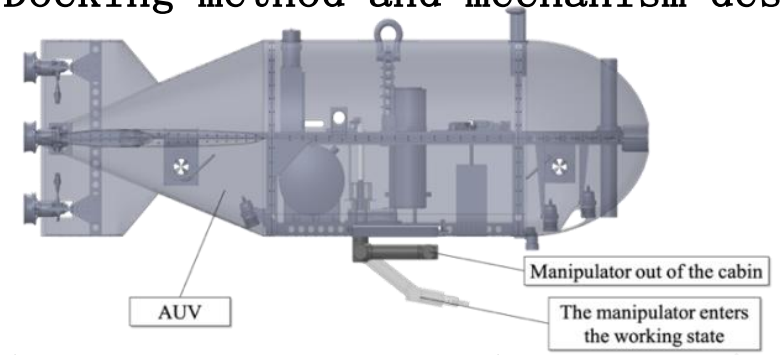

Schematic of AUV－manipulator system

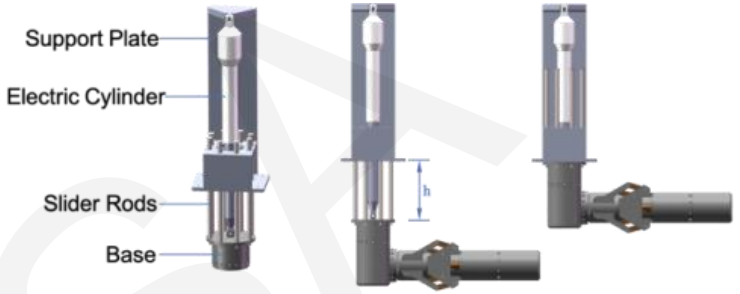

Schematic of manipulator lifting mechanism

Since there is a stowage compartment for the robotic arm inside the AUV, it is necessary to design the lifting mechanism to achieve the switching of the operational auv between the range mode and the operational mode.

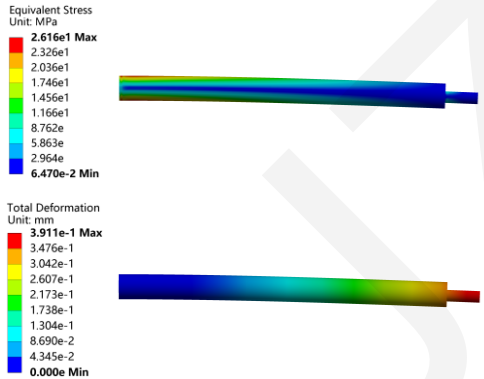

Static finite element analysis of sliding rod

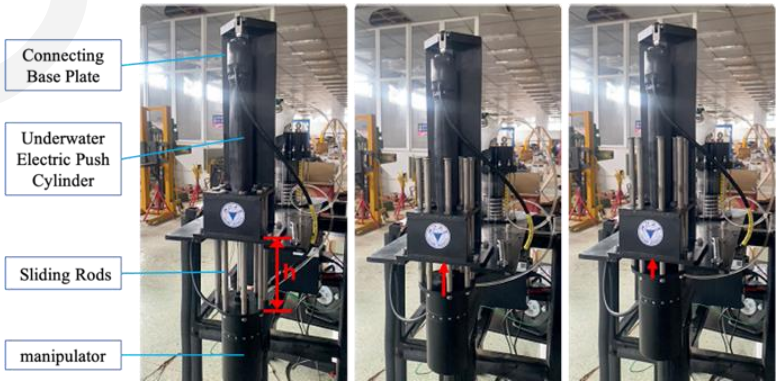

Display of the working process of the lifting mechanism

The lifting mechanism consists of an underwater electric push cylinder, a sliding rod, and a connecting base plate, etc. The electric push cylinder on the telescopic mechanism pushes the manipulator to move upward or downward.

Kinematic analysis

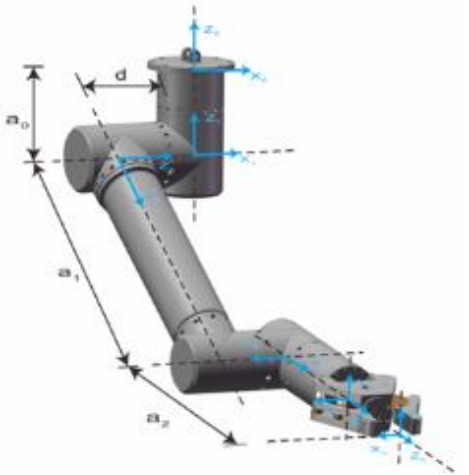

12 4-DoF configuration and DH convention

Simplified DH parameters

	θ	d	a	α
1	0	0	0	π/2
2	0	0	0.414	0
3	0	0	0.253	π/2

$$^{i-1}\boldsymbol{A}_i = \begin{bmatrix} c_i & -c\alpha_i s_i & s\alpha_i s_i & a_i c_i \\ s_i & c\alpha_i c_i & -s\alpha_i c_i & a_i s_i \\ 0 & s\alpha_i & c\alpha_i & d_i \\ 0 & 0 & 0 & 1 \end{bmatrix}$$

$$^{0}\boldsymbol{A}_1 = \begin{bmatrix} c_1 & 0 & s_1 & 0 \\ s_1 & 0 & -c_1 & 0 \\ 0 & 1 & 0 & 0 \\ 0 & 0 & 0 & 1 \end{bmatrix}$$

$$^{1}\boldsymbol{A}_2 = \begin{bmatrix} c_2 & -s_2 & 0 & a_2 c_2 \\ s_2 & c_2 & 0 & a_2 s_2 \\ 0 & 0 & 1 & 0 \\ 0 & 0 & 0 & 1 \end{bmatrix}$$

$$^{2}\boldsymbol{A}_3 = \begin{bmatrix} c_3 & 0 & s_3 & 0 \\ s_3 & 0 & -c_3 & 0 \\ 0 & 1 & 0 & 0 \\ 0 & 0 & 0 & 1 \end{bmatrix}$$

$$^{0}\boldsymbol{A}_3 = {}^{0}\boldsymbol{A}_1\,(\theta_1)\,{}^{1}\boldsymbol{A}_2(\theta_2)\,{}^{2}\boldsymbol{A}_3(\theta_3) =$$

$$\begin{bmatrix} c_1c_2c_3 - c_1s_2s_3 & s_1 & c_1c_2s_3 + c_1s_2c_3 & c_1c_2a_2 \\ s_1c_2c_3 - s_1s_2s_3 & -c_1 & s_1c_2s_3 + s_1s_2c_3 & s_1c_2a_2 \\ s_2c_3 + c_2s_3 & 0 & s_2s_3 - c_2c_3 & a_2s_2 \\ 0 & 0 & 0 & 1 \end{bmatrix}$$

In this paper, inverse kinematic equations based on positive kinematics are used to mathematically describe the mapping relationship between the joint angles and end positions of the manipulator.

Kinematic analysis

Working volume of the robotic arm's configuration for prototyping and testing

θ	Max	Min
θ_1	π	π
θ_2	0	-π/2
θ_3	π/3	-π/3

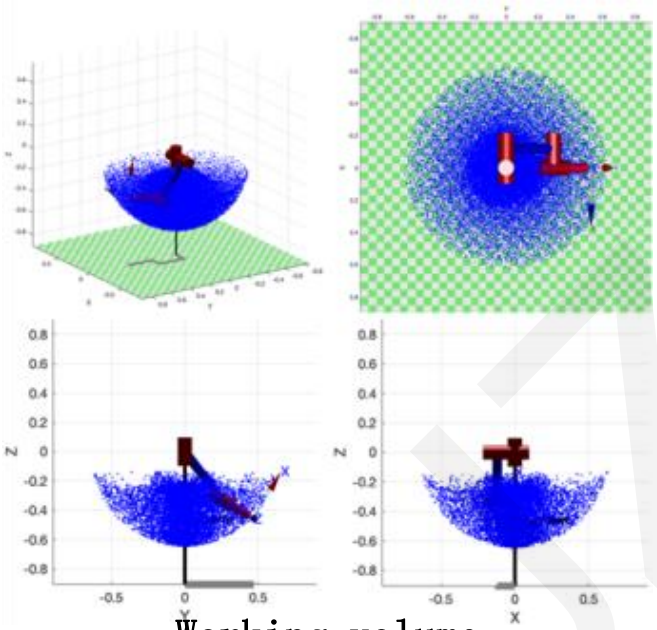

Working volume

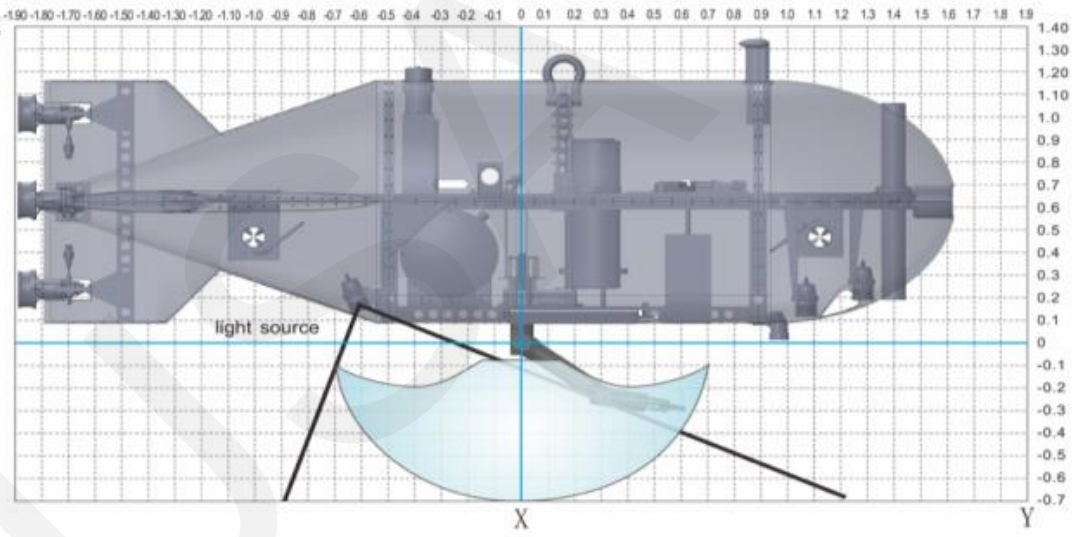

Schematic of UVMS system workspace

The Monte Carlo method of generating random numbers is used to find the point cloud map of the working space of the robotic arm on the basis of positive kinematics equations, and only the position within this space can be a valid target point of the robotic arm.

Experiment andConclusions

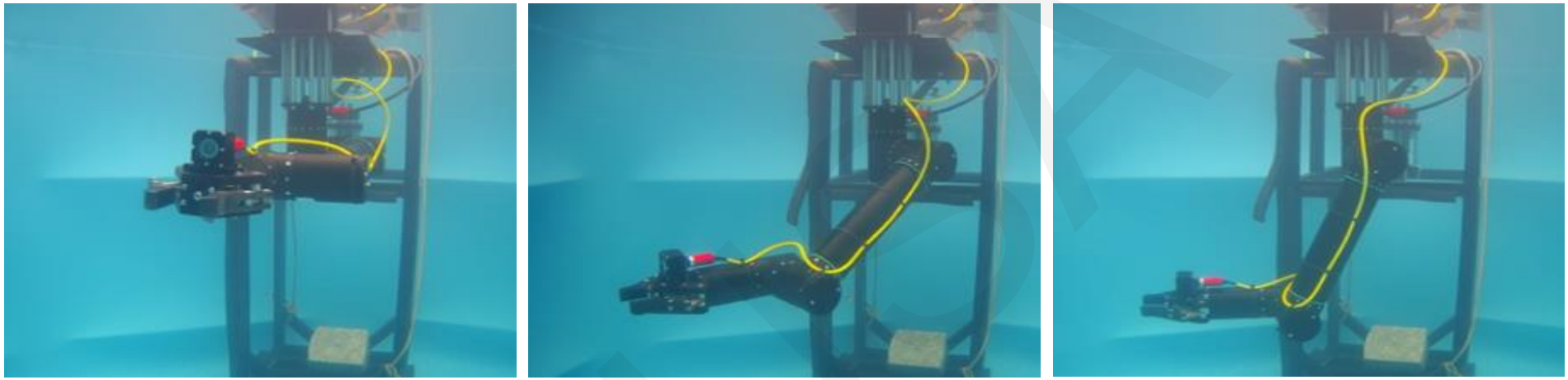

Underwater experiment of manipulator: (a), (b), and (c) shows the initial, middle, and end poses of the trajectory running for one cycle, respectively.

The experimental data of the above-water and underwater experiments are compared. By comparison, it can be concluded that the manipulator joints operate more stably in the uniform acceleration/deceleration process, with a trace overshoot at the transition from uniform deceleration to a stop. In the uniform speed process, the joint angle tracking is unstable, and the error range is approximately 0.01 rad, as shown by the fluctuation amplitude.

Experiment andConclusions

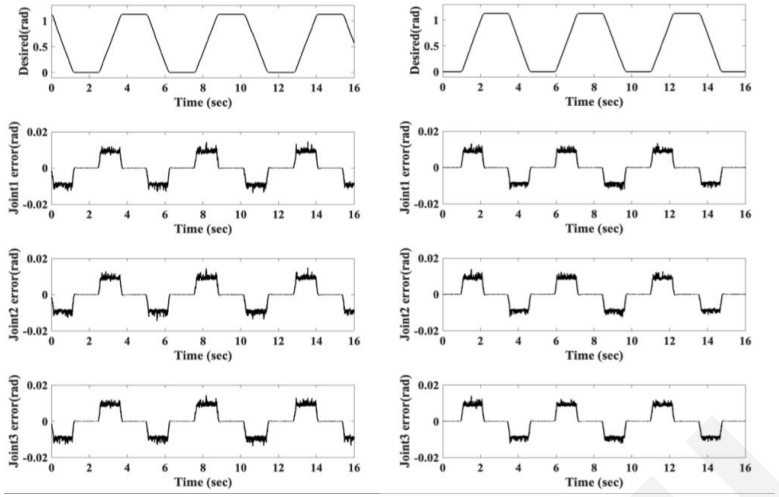

Angle tracking error of each joint. In air (a) and water (b)

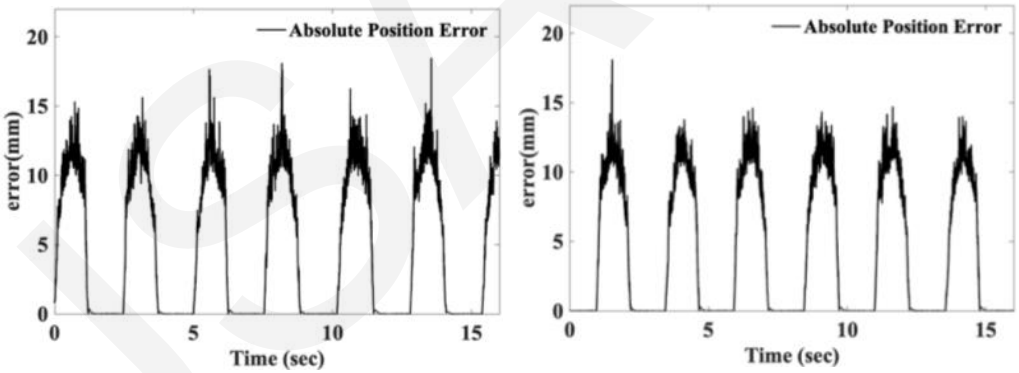

Space motion trajectory error of the end-effector of a manipulator. In air (a) and water (b)

Further analyzes the motion trajectory error of the manipulator actuator. By comparison, it can be concluded that the average peak of the absolute tracking error of the manipulator in air is approximately 18 mm, whereas that underwater is approximately 14 mm. The end motion accuracy of the manipulator underwater is higher than that in water, and the amplitude of the vibration generated during the uniform speed is also smaller than that during air operation.